Vol. 47, No. 3 (2025) 583-592, DOI: 10.24874/ti.1935.04.25.07

Tribology in Industry

www.tribology.rs

RESEARCH

Features of Wear Resistance in Tribological Contacts with Textured Surfaces under Boundary Friction Conditions

Volodymyr Marchuk[a,b,*], Gennady Lavanov[a,b], Miroslav Kindrachuk[a], Oleh Harmash[a,b], Olena Klymuk[b]

[a]State University "Kyiv Aviation Institute", Kyiv, Ukraine,
[b]National Technical University of Ukraine "Igor Sikorsky Kyiv Polytechnic Institute", Kyiv, Ukraine.

Keywords:

Mathematical model
Lubricant droplet
Wear resistance
Stress-strain state
Boundary friction
Textured surface
Dimple

* Corresponding author:

Volodymyr Marchuk
E-mail: sunduk_2005@ukr.net

Received: 14 April 2025
Revised: 6 June 2025
Accepted: 7 July 2025

A B S T R A C T

The features of wear resistance of tribological contacts with a textured surface under boundary friction conditions have been investigated. A mathematical modeling of the behavior of the lubricant in the dimple was conducted, considering the influence of inertial forces. It is shown that the dynamics of the "oil droplet" depend on the value of the parameter α, which represents linear acceleration. A critical value of the parameter $\alpha<0$ was established, below which additional wetting of the tribocontact surface with oil from the dimple becomes impossible. At $\alpha=0$, the process of additional wetting with oil is determined solely by the oil droplets particles located near the dimple surface. At $\alpha>0$, oil particles leave the dimple and contribute to the regeneration of the boundary lubricant film. Experimental studies on the wear resistance of tribological contacts with a textured surface under boundary friction conditions have been carried out. High wear resistance of textured surfaces, additionally reinforced by ion-plasma thermocyclic nitriding, has been established. These surfaces exceed the wear resistance of other samples by 1.45–3.0 times due to stress redistribution, higher mechanical properties of the surface layer that inhibit defect formation in the tribocontact surface layer, and the high protective effect of the boundary lubricant film.

1. INTRODUCTION

Modern technological methods of surface strengthening open significant possibilities for the creation of protective structures for tribotechnical applications. They ensure the reliable operation of friction units under various operating conditions, enhance productivity, and consequently lead to substantial savings in material, energy, and labor resources. Today, technological methods for creating textured (discrete) surfaces offer extensive opportunities. The essence of these methods lies in replacing the traditional continuous surface layer with a discontinuous mosaic-discrete structure. Discrete surfaces, as a means of improving the tribological characteristics of machine parts and assemblies, have existed for many years but have gained widespread popularity in the last decade as the most promising and viable direction in surface engineering. The implementation of such technology expands the operational range of parts under extreme conditions in terms of permissible load, wear resistance, friction coefficient, and physico-mechanical-chemical characteristics of friction pairs. The wear mechanism of machine parts and assemblies with a textured structure is complex and varies for different friction units. Most friction units operate under lubricated conditions and require continuous improvement in their lubrication mechanism. Therefore, research aimed at a deeper understanding of the physical processes involved in the lubrication mechanism of textured surfaces under boundary friction conditions remains relevant.

Studies on the influence of surface texture on the lubricating characteristics of fluid-film bearings began in the early 20th century. The first works in this field were conducted by Falts K. in 1929, who proposed creating lubricant supply channels in stationary bearing elements. He recommended groove inclination angles of 0.5% for high speeds with low pressure and 0.2% for low speeds with high pressure [1]. In the 1960s, Hamilton and Allen [2] noted that the "irregularities and depressions" formed on the face seal of a rotating shaft create hydrodynamic pressure, improving load-bearing capacity. These initial studies prompted further analytical and experimental research in various countries on the efficiency of surface texture under lubricated contact conditions and on establishing the lubrication mechanism within the dimples of textured surfaces.

The most significant wear occurs at minimal lubricant film thickness and under limited lubricant supply (boundary friction regime). Various theories exist regarding the mechanism of boundary lubrication. The self-organization of lubricant films is discussed in numerous studies [3-5]. However, most researchers agree that under boundary lubrication, the processes of film destruction and restoration at contact points play a crucial role, and the restoration rate must not be lower than the destruction rate [6-9].

The physical properties of the surface layer of the material, where a unique micro-relief forms, significantly influence the adhesion and lubricity of surfaces in tribological contacts. Different grains of the surface have different surface tension coefficients and fields. The surface field of a metal varies between sharp protrusions and flat areas of the sub- and micro-relief. Thus, the monomolecular lubricant layer will exhibit different adhesion properties at different points on the surface [10-12].

In [13], it is noted that, along with traditional processes of secondary structure formation and destruction, the excitation of internal magnetic fields plays a crucial role in determining the wear mechanism of textured surfaces. An inhomogeneous resultant magnetic field forms at the edges of discrete areas, leading to the emergence of ponderomotive force. This force acts on wear particles, directing them toward areas of higher magnetic field induction – the dimple edges and further into the dimple preventing unacceptable contact surface destruction processes.

Many studies focus on the effect of external electromagnetic radiation on the tribosystem. Work [14] presents research results on a support bearing lubricated with a magnetorheological fluid activated by a localized constant magnetic field to control the lubricant film thickness. A reduction in magnetic field intensity at high speeds decreases the viscosity of the lubricant fluid, thereby reducing friction losses.

The authors of [15] developed a mathematical model of the lubrication mechanism for textured surfaces (dimples) under boundary friction conditions. They established that for effective lubrication in tribocontacts experiencing boundary film destruction, the rotational speed of the sample must be $n > 27$. This ensures lubricant transfer from the dimple to the problem zone, restoration of the boundary lubricant film on the tribocontact surface, and uninterrupted operation of the tribological unit.

Experimental and numerical studies have shown that microtextures act as tiny lubricant reservoirs that supply lubricant to tribocontacts under mixed or boundary lubrication conditions. It has been proven [16,17] that friction reduction occurs when the texture size remains smaller than the Hertzian contact dimensions, whereas friction increases when the texture elements are equal to or larger than the Hertzian contact size. It is also important to note that micro-defect depth is a critical design parameter for improving fatigue durability of the contact [18].

Numerous studies have examined the effect of the initial surface area dimensions on its wear resistance. It has been demonstrated that the density of micro-reservoir placement should be maximized, and the micro-dimple dimensions should be optimized. A formula for determining the optimal groove depth and spacing was derived, indicating that groove depth can be reduced by decreasing the spacing between grooves [19]. Additionally, an optimal ratio between the initial surface segment dimensions and the width of artificially created micro-dimples was identified. The optimal micro-dimple area should be approximately 30% of the total friction surface area [20,21].

Thus, the selection of optimal texture design parameters makes it possible to influence the lubricating ability, reduce the running-in duration, and improve the tribological performance of tribological contacts. This is particularly important for critical and heavily loaded components and mechanisms operating under limited lubricant supply conditions [22,23].

Mechanisms for increasing load-bearing capacity have been described, including increasing hydrodynamic pressure on the surface texture [24], applying additional lubricants to the actual contact area via the suction-intake effect [25], reducing the actual contact area [26], retaining lubricants through the reservoir effect [27], and removing wear particles [28].

Kango et al. [29] studied textured sliding bearings using the generalized Reynolds equation. Their model accounts for viscous heat dissipation, non-Newtonian lubricant behavior, and incorporates a mass-conserving cavitation algorithm based on the Jakobsson-Floberg-Olsson (JFO) boundary conditions. Han et al. [30] used a modified averaged Reynolds equation to study the effects of misalignment and axial shaft motion on the performance of sliding bearings with rough surfaces under transient and mixed lubrication conditions.

Thus, the wear mechanism of textured surfaces under boundary friction is complex, depends on numerous factors, and requires further detailed investigation.

2. OBJECTIVES

The aim of this study is to develop a mathematical model describing the behavior of lubricant between contacting surfaces and inside dimples to determine the lubrication mechanism of tribological contacts with a textured dimple surface under boundary friction conditions, as well as to conduct experimental research. This will provide a deeper understanding of the lubricant's action in boundary friction conditions and facilitate the development of measures to improve lubrication, ultimately enhancing the wear resistance of tribological contacts with textured surfaces.

3. THE STUDY MATERIALS AND METHODS

Experimental studies on the tribotechnical characteristics of textured surfaces were conducted under friction conditions with limited lubricant supply, in accordance with the recommendations of GOST 26614-85, which defines the test method for antifriction powder materials to evaluate their tribological properties under friction conditions with limited lubricant supply. The standard establishes the methodology for determining the dependence of wear and friction force on sliding speed and applied load, as well as for calculating wear rate and the coefficient of friction.

Hardened 45 steel was used as the counterbody material, while the sample material was high-strength alloy structural steel 30KhGSA, also hardened, belonging to the group of chromium–manganese–silicon alloys. The chemical composition of the steel includes: Cr (0.8–1.1%), Mn (0.8–1.1%), Si (0.9–1.2%), C (0.28–0.34%), Ni (up to 0.30%), Cu (up to 0.30%), S (up to 0.035%), P (up to 0.035%), Al (up to 0.05%), V (0.05–0.12%), Mo (0.15–0.25%).

The textured surface in the form of dimples was formed on the working surface of the specimen by means of plastic deformation under the dynamic action of an indenter using a special device [31], which enables control over the geometry of the dimples, the spacing between dimples, and the spacing between rows. The geometric properties of the textured surface were as follows: row spacing X1 = 2.0×10^{-3} m, dimple spacing within a row X2 = 2.0×10^{-3} m, and dimple depth = 1.5×10^{-3} m – selected to minimize residual tensile stresses (Fig. 1).

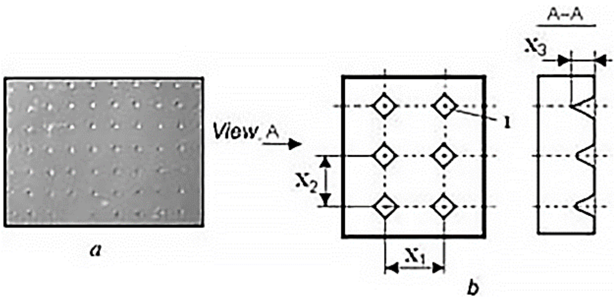

Fig. 1. Discrete surface: a – general view; b – schematic arrangement of dimples.

The textured surface was further strengthened by ion-plasma thermocyclic nitriding (IPTN) [32].

To test discrete surfaces under boundary friction conditions, the M-22M friction machine was used. The friction pair contact followed the "disk-pad" scheme. Industrial lubricant I-20 was used as the lubrication medium, in accordance with GOST 20799-75. A lubrication device was applied to ensure boundary friction conditions, following the recommendations of GOST 26614-85, which sets the technical specifications for industrial oils and regulates the requirements for their quality. The experiments were conducted at a sliding speed of 0.625 m/s, a specific load of 10.0 MPa, and a sliding distance of 2000 m. Industrial lubricant I-20A was used as the lubricating material, in accordance with GOST 20799-75.

Numerical modeling of the stress-strain state of textured surfaces was performed using the finite element method (MSC Visual Nastran for Windows). To assess the influence of the specified factors, a finite element model was developed to simulate the stress–strain state of the specimen under external loading. To simplify the calculation, a segment of the model was considered and discretized into hexagonal finite elements. The size of the finite elements ranged from 75 to 140 μm.

For the model without dimples, the number of nodes was 44,590 and the number of elements was 39,936; for the model with dimples, the corresponding values were 49,966 nodes and 46,176 elements. The application of forces and constraints in the finite element model corresponded to the scheme shown in Fig. 2. The notations used in Fig. 2 are as follows: H = 2 mm, L = 8 mm, h_1 = 300 μm, h_2 = 150 μm, distance between dimples = 2 mm.

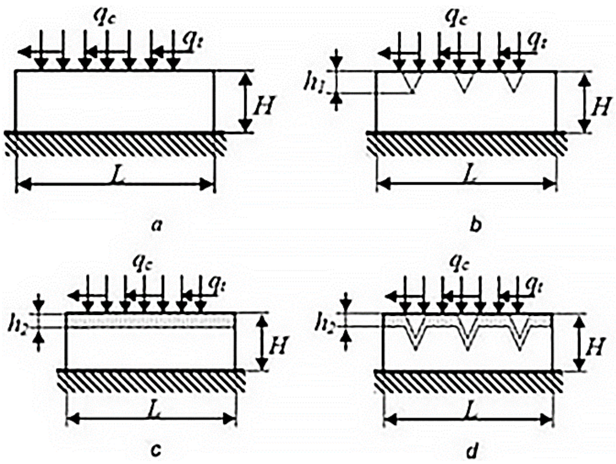

Fig. 2. Schematic application of loading to the models: a – 30KhGSA hardened; b – 30KhGSA with dimples; c – 30KhGSA with coating; d – 30KhGSA with dimples and coating; qc – distributed compressive load; qt – tangential (shear) load; L – model width; H – model height; h_1 – dimple depth; h_2 – coating thickness.

The base of the model was rigidly fixed, while the surface was subjected to a resultant load combining tangential and normally applied distributed forces. To ensure a consistent loading level across all models, the surface nodes of each model were associated with a surface constructed from four reference points. This surface was then subjected to a distributed compressive load (qc = 1000 N/m^2) over the area of the frictional contact, along with a tangential load (qt = 100 N/m^2).

To investigate the lubrication behavior between the contacting surfaces and within the dimples, the motion of an oil droplet inside a dimple is considered (Fig. 3). Let the space between the contacting surfaces be filled with a homogeneous lubricant. The counterbody, having a larger radius of curvature, is smooth, while the second body – the specimen with a smaller radius – contains various recesses (dimples), which are arranged periodically. Let the space between two coaxially rotating cylinders be filled with a homogeneous oil. The upper cylinder, which has a larger radius of curvature, is smooth, while the lower cylinder (with a smaller radius) contains various dimples, periodically arranged. It is assumed that the depth of these dimples is not very large and that they have a conical shape (triangular cross-section profile). The homogeneity of the oil filling the space implies the absence of density and temperature gradients. In other words, heat exchange processes will be neglected, assuming that no heating of the cylinders occurs during rotation.

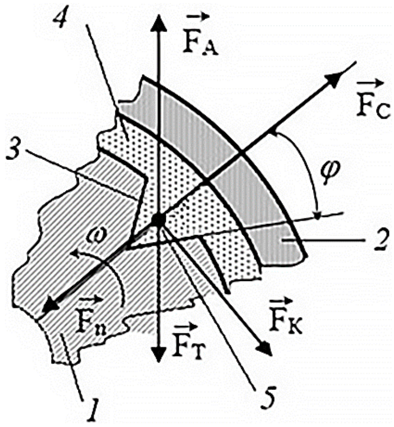

Fig. 3. Schematic representation of the motion of a lubricant droplet and the forces acting on it during boundary lubrication: 1 – specimen; 2 – counterbody; 3 – dimple; 4 – lubricant; 5 – lubricant droplet.

A selected oil droplet located inside a dimple is affected by the following forces: *gravitational force* $F_T = \Delta mg$ (Δm – mass of the oil droplet, kg; g – acceleration due to gravity, m/s^2), directed vertically downward. Since the oil droplet is in contact with the sample surface (a solid body), *surface tension force* acts between the two media – $F_n = \sigma l$ (σ – surface tension coefficient; l – length of the inclined part of the dimple, m), the oil wets the surface.

Next, *Archimedean force* $F_A = \rho g \Delta V$ (ρ - oil density, kg/m^3; ΔV – volume of the oil droplet, m^3), which tends to push the droplet upward. Since convection (mixing) is absent in the oil, this means that the Archimedean force compensates for the gravitational force. In a rotating system, as known from general physics, two additional forces arise: *centrifugal force* $F_c = \Delta m\omega^2 r$ (ω – angular velocity, s^{-1}; r – radius vector indicating the position of the droplet with mass Δm, m), which tends to "eject" the droplet outward, and *Coriolis force* $F_k = 2\Delta m\omega\upsilon$ (υ – linear velocity of the oil droplet), which attempts to alter the trajectory of the droplet's motion without changing its speed magnitude, since the droplet participates in two types of movement (translational along the dimple and rotational motion).

4. RESULTS AND DISCUSSION

4.1 Results of mathematical modeling of lubricant behavior

Let us consider the dynamics of an oil droplet located in a dimple. To do this, we isolate an infinitesimal volume of oil droplet with mass Δm and apply Newton's second law to this mass in Cartesian coordinate projections (as shown in Fig. 1):

$$\begin{cases} \Delta m \dfrac{dv_x}{dt} = (F_c - F_n)\mathrm{Cos}(\omega t); \\ \Delta m \dfrac{dv_y}{dt} = (F_A - F_T) + (F_c - F_n)\mathrm{Sin}(\omega t), \end{cases} \quad (1)$$

The system (1) is supplemented with the Coriolis force, as the translational motion of mass Δm is superimposed with rotational motion:

$$\begin{cases} \Delta m \dfrac{dv_x}{dt} = (F_c - F_n)\mathrm{Cos}(\omega t) + F_k^{(x)}; \\ \Delta m \dfrac{dv_y}{dt} = (F_A - F_T) + (F_c - F_n)\mathrm{Sin}(\omega t) + F_k^{(y)} \end{cases}, \quad (2)$$

where $F_k^{(x)} = 2\Delta m\omega v_y, F_k^{(y)} = -2\Delta m\omega v_x$. Since the system is homogeneous, the first term on the right-hand side of the second equation in (2) equals zero. Then, after simple transformations, system (2) takes the form:

$$\begin{cases} \dfrac{dv_x}{dt} = \alpha\,\mathrm{Cos}(\omega t) + 2\omega v_y; \\ \dfrac{dv_y}{dt} = \alpha\,\mathrm{Sin}(\omega t) - 2\omega v_x \end{cases}, \quad (3)$$

where parameter $\alpha = \omega^2 r - \dfrac{\sigma l}{\Delta m}$. The solution to system (3) for an arbitrary value of parameter α has the form:

$$\begin{aligned} v_x &= A\mathrm{Sin}(2\omega t + \varphi_0) + \frac{2}{3}\frac{\alpha}{\omega}\mathrm{Sin}(\omega t), \\ v_y &= A\mathrm{Cos}(2\omega t + \varphi_0) - \frac{1}{6}\frac{\alpha}{\omega}\mathrm{Cos}(\omega t). \end{aligned} \quad (4)$$

where parameter A – the velocity amplitude and φ_0 - the initial phase. Using (4), it is easy to derive an equation (in parametric form) for the velocity value:

$$v = \sqrt{v_x^2 + v_y^2} \quad (5)$$

To obtain expressions for the particle trajectory, the equations from system (4) should be integrated. By performing integration, we obtain the general case:

$$\begin{cases} r_x = \dfrac{R}{2}\left(1-\mathrm{Cos}(2\omega t)\right) + \dfrac{2}{3}\dfrac{\alpha}{\omega^2}\left(1-\mathrm{Cos}(\omega t)\right) \\ r_y = \dfrac{R}{2}\mathrm{Sin}(2\omega t) - \dfrac{1}{6}\dfrac{\alpha}{\omega^2}\mathrm{Sin}(\omega t). \end{cases} \tag{6}$$

where R – the sample radius. System (6) allows for analysis of the particle trajectory.

Let us consider the first limiting case, where parameter $\alpha > 0$. This case implies (as seen from the definition) that the surface tension force is weaker than the centrifugal force, i.e., the condition $F_c > F_n$ is satisfied. Under this condition, the oil droplet of mass Δm will tend to move with velocity v_y. The dependence of horizontal v_x and vertical v_y component of velocity on time (from the initial moment of motion up to ¼ of the period) is shown in Fig. 4.

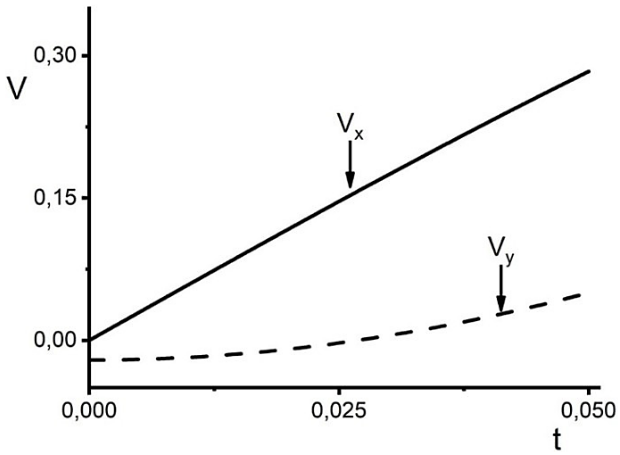

Fig. 4. Dependencies of horizontal velocity v_x (blue line) and vertical velocity v_y (red line) on time for the case $F_c > F_n$ ($\alpha > 0$).

From Fig. 4, it is evident that the velocity of motion v_x continuously (linearly) increases throughout the time interval, starting from zero, while the vertical velocity component v_y, starts at a certain negative value, gradually increases while remaining negative up to approximately 1/8 (0.027 s) of the period, and then becomes positive.

The dependence of the velocity modulus (5) on time for this case is shown in Fig. 5. The figure shows that initially, when the system starts rotating, the oil droplet moves uniformly (without acceleration), corresponding to a small horizontal section, and then begins to move with constant tangential acceleration, corresponding to the linear section of the graph.

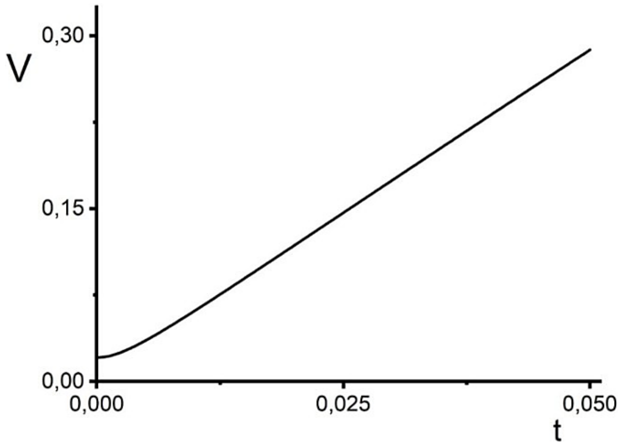

Fig. 5. The dependence of velocity modulus on time for the condition $F_c > F_n$ ($\alpha > 0$).

Now, let us analyze system (6). Systems (6) and (4) both represent parametric equations describing the particle trajectory. However, obtaining an analytical expression for the trajectory $y(x)$ is impossible due to the strong nonlinearity of the equations. Nevertheless, numerical methods allow for an effective workaround to these difficulties.

The dependence r_x, r_y from (6) for this case is shown in Fig. 6. As seen in the figure, the vertical coordinate r_y changes linearly over time (with a constant velocity), whereas the horizontal coordinate r_x exhibits a nonlinear behavior at small times (about 1/8 of the period) and only later follows an almost linear trend.

Now, let us consider the second limiting case, where $\alpha = 0$. This case (see system (3)) shows that the surface tension force exactly compensates for the centrifugal force. Although system (3) has a solution, it is determined only by the additional Coriolis force terms, and the additional wetting process is governed solely by oil particles near the dimple surface, contradicting the model.

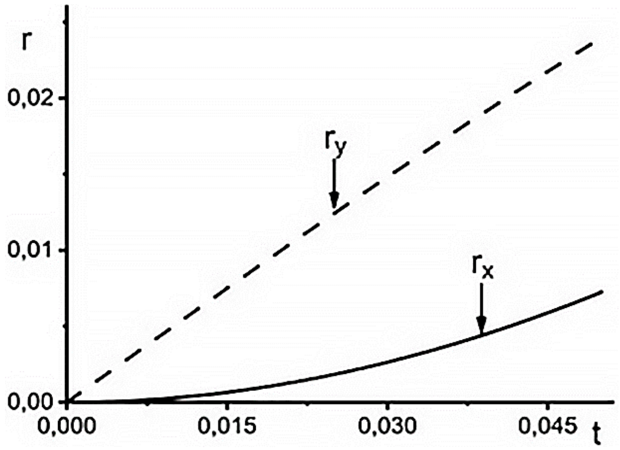

Fig. 6. The dependence of horizontal r_x and vertical r_y coordinate on time for the condition $F_c > F_n(\alpha > 0)$.

However, this case is crucial for determining the critical rotation frequency based on the type of oil and material. To do this, we turn to the definition of this coefficient:

$$\alpha = \omega^2 r - \frac{\sigma l}{\Delta m} = 0 \Rightarrow \omega_c = \sqrt{\frac{\sigma l}{\Delta m r}}.$$

From the last expression, it is clear that the critical rotation frequency depends on qualitative parameters (surface tension coefficient σ), which characterize the liquid (oil).

The third limiting case occurs when $\alpha < 0$. This case is characterized by the dominance of the surface tension force over the centrifugal force, preventing the oil droplet from leaving the bottom of the dimple and initiating motion. Although system (3) has a solution in this case, it has no physical meaning.

It should also be noted that the criterion for the oil droplet to leave the dimple is the fulfillment of the condition:

$$r_y > l'$$

where l' – is the cone (dimple) height, which can be determined from the simple relation $l' = l / \mathrm{Cos}(\varphi / 2)$, where φ is the cone angle (at the apex). It follows that the thinner the dimple, the smaller the angle, and in the limiting case $\varphi \to 0, l' \to l$.

Figure 7 shows the trajectory of the oil droplet for two different rotation frequencies. Curve 1 (which has no physical meaning) corresponds to the case of a negative value $\alpha < 0$, i.e., when the frequency is below the critical value. Curve 2 corresponds to the condition $\alpha > 0$ when rotation frequency exceeding the critical value.

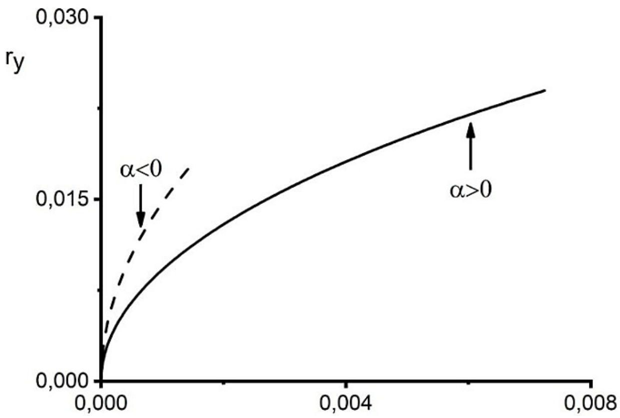

Fig. 7. Dependence of oil particle trajectories at different rotation frequencies: 1 – rotation frequency below critical; 2 – rotation frequency above critical.

4.2. Experimental studies of textured surfaces under boundary lubrication conditions

Experimental studies of the tribological characteristics of textured surfaces have shown that the highest wear resistance is exhibited by samples with a textured surface additionally strengthened by the IPTA method (Table 1), which exceed the wear resistance of other samples by 1.45–3.0 times.

Table 1. Tribotechnical characteristics of textured surfaces under boundary friction conditions.

Material	Wear, mg/km	Coefficient of Friction
30KhGSA	3,1	0,12
30KhGSA+IPTN	2,14	0,091
30KhGSA+dimples	1,16	0,07
30KhGSA+dimples+ IPTN	1,01	0,078

The high wear resistance of the textured surface is associated with the strong protective effect of surface-nitrided layers and their high hardness, which enhances the defect inhibition effect in the surface layers of contacting surfaces, reduces the intensity of wear product formation in the surface layer, and prevents damage marks on the friction surface. Additionally, the high wear resistance of the textured surface is explained by the high efficiency of the lubrication action of the texture, which accelerates the wetting processes of actual tribocontact areas and the regeneration of the boundary lubricant film.

The analysis of the structure of the nitrided layers revealed the presence of carbonitride phases $Fe_{2\text{-}3}$(NC) and Fe_3(N,C), on the surface of the nitrided coating, as well as a small amount of the α-Fe(NC) solid solution, which ensures high microhardness values of the nitrided layers. The formation of carbonitride phases is explained by the specifics of the IPTA technological process, where carbon in the form of propane C_3H_8 is introduced into the saturating mixture (Table 2).

Table 2. Results of the layer-by-layer X-ray structural analysis of the nitrided textured coating.

Layer depth from the sample surface, μm	Amount of nitrogen, wt. %	Phase composition of the layer
10	7,04	$Fe_{2\text{-}3}$ (N,C), Fe_3(N,C), α-Fe(NC), Fe_4N
40	3,98	α-Fe(N), $Fe_{2\text{-}3}N$, Fe_4N
70	0,60	α-Fe(N), Fe_2N
100	0,42	α-Fe(N)
130	0, 01	α-Fe(N)

As the depth of the nitrided coating increases, the amount of carbonitride phases decreases.

The strengthening of the surface layer by the IPTA method, both for the initial and the textured surface, leads to a 20–30% increase in the level of equivalent stress distribution. However, since the yield strength of the nitrided layer is higher than that of the base material, the increased stress state in the nitrided material does not reduce the strength characteristics of the component. The presence of dimples has little effect on the stress state of the surface layer, but at a distance from the surface beneath the dimples, stresses decrease by 40%, thus unloading the base material (Fig. 8).

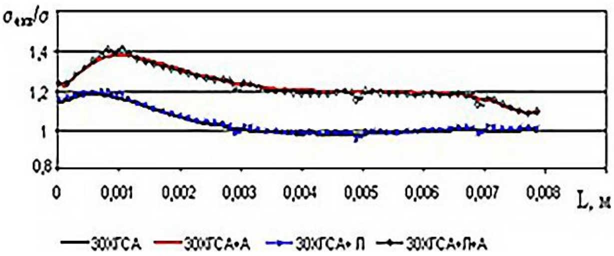

Fig. 8. Distribution graph of relative equivalent stresses in the surface layer of the element along its length (σ – maximum stress of the initial element).

Considering the stress state along the depth (thickness) of the element, it is evident (Fig. 9) that there is a significant stress gradient of approximately 21–28% between the nitrided surface and the base material. As shown in the graph, the nitrided layer unloads the base material, which has a lower yield strength, thereby increasing the overall service life of the entire component (structure).

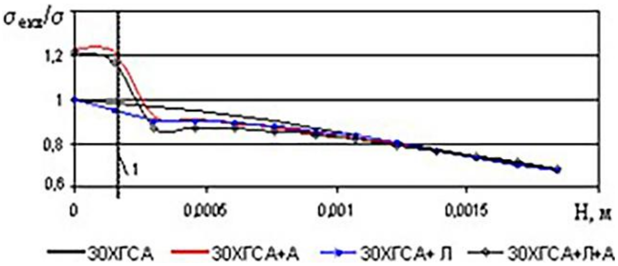

Fig. 9. Distribution graph of relative equivalent stresses along the depth of the component along the Y-axis (0 corresponds to the surface of the specimen; 1 indicates the boundary between the nitrided and non-nitrided material layer).

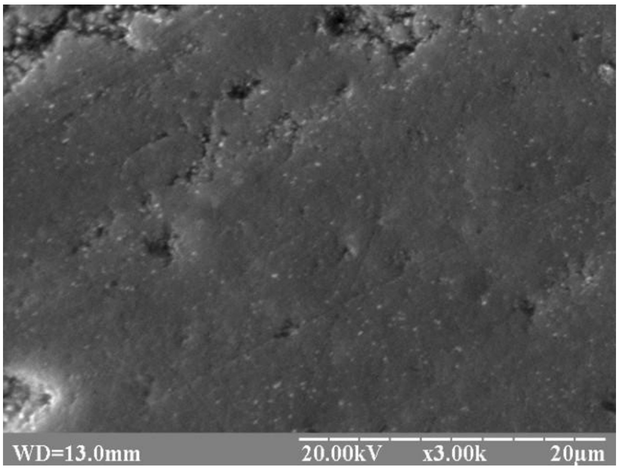

(a)

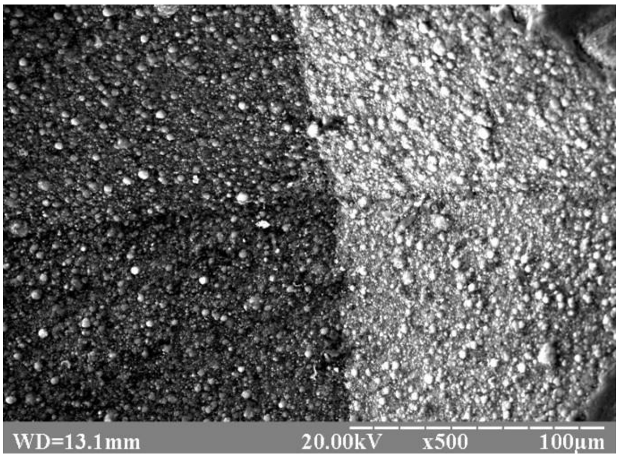

(b)

Fig. 10. Micrographs of the friction surface of the textured surface strengthened by the IPTN method (30KhGSA+D+C) under boundary lubrication conditions: a – friction surface in front of the dimple; b – bottom of the dimple.

Thus, experimental studies on wear resistance under boundary lubrication conditions demonstrated a relatively high durability of the nitrided specimens with dimples, without delamination or cohesive cracking of the surface layers (Fig. 10). This is attributed to the strong protective effect of the nitrided surface layers, which leads to a reduction in the intensity of wear product formation within the surface layer.

The stress gradient between the base material and the nitrided layer does not reduce the strength characteristics of the component under contact and friction conditions. The high wear resistance of the nitrided layer itself and its resistance to cracking, which usually occurs through cohesive delamination of the substrate and coating, can be explained by the fact that the nitrided surface modification does not represent a coating of the substrate with another material having sharply different properties. As shown in Table 2, a gradual transition of the structural composition of the nitrided layer is observed, with a high content of carbonitride compounds near the surface, which gradually decreases with depth. This creates a smooth decline in deformation resistance characteristics and prevents high property gradients.

5. CONCLUSION

1. The dynamics of oil droplet behavior in a dimple, considering the influence of inertial forces, have been analyzed, expanding the understanding of the wear mechanism of textured surfaces under boundary friction conditions. It has been shown that the rotational speed affects the dynamics of the oil droplet within the dimple. There exists a critical value of the parameter $\alpha<0$, dependent on the rotational frequency of the sample, below which additional wetting of the tribocontact surface becomes impossible. At $\alpha=0$, the process of additional wetting with oil is determined solely by oil particles located near the dimple surface. At $\alpha>0$, oil particles leave the dimple, ensuring the wetting of the tribocontact surface and the regeneration of the boundary oil film. The trajectory of an oil particle is complex and oscillatory; however, within a time interval of up to ¼ of the period, the motion trajectory of the oil particle is nonlinear and follows a power function.
2. High wear resistance under boundary friction conditions has been established for textured surfaces additionally strengthened by ion nitriding, exceeding the wear resistance of other samples by 1.45–3.0 times. This effect can be explained by several factors. Firstly, the strong protective effect of the surface-nitrided layers and their high hardness enhances the defect inhibition effect in the surface layers of contacting surfaces, reducing the intensity of wear product formation. Secondly, the high efficiency of the lubrication action of the texture accelerates the wetting processes at actual tribocontact points and the regeneration of the boundary lubricant film. Thirdly, the presence of a nitrided surface layer improves the condition of the sample surface, redistributes stresses due to the higher mechanical properties of the surface layer and their gradual decrease with depth, proportionally adjusting the properties and stress distribution of the material with the textured surface. This combination ultimately enhances wear and damage resistance.

REFERENCES

[1] K. Falts, *Racionalnye smazochnye kanavki v podshipnikah*, Moscow–Leningrad: Gosizdat, 1929.

[2] D. B. Hamilton, J. A. Walowit, and C. M. Allen, "A Theory of Lubrication by Microirregularities," *Journal of Basic Engineering*, vol. 88, no. 1, pp. 177-185, Mar. 1966, doi: 10.1115/1.3645799.

[3] B. Kostetsky, M. Natanson, and L. Bershadsky, *Mekhanokhimicheskie protsessy pri granichnom trenii*, Moscow: Nauka, 1972.

[4] V. Shevelya, and G. Kalda, *Fretting-ustalost' metallov*, Podillya, 1998.

[5] A. Akhmatov, *Molekulyarnaya fizika granichnogo trenia*, Moscow: Gosudarstvennoe izdatel'stvo fiziko-matematicheskoi literatury, 1963.

[6] Yu. Rozenberg, *Vliyanie smazochnykh masel na nadezhnost' i dolgovechost' detalei mashin*, Moscow: Mashinostroenie, 1970.

[7] P. Matveevsky, I. Buyanovsky, and O. Lazovskaya, *Protivozadirnaya stoikost' smazochnykh sred pri trenii v rezhime granichnoi smazki*, Kyiv: Nauka, 1978.

[8] G. Fuks, "Adsorbtsiya i smazochnaya sposobnost' masel," *Trenie i iznos*, vol. 4, no. 3, pp. 398–414, 1983.

[9] N. Gitis, "O roli mikrogeometrii v razvitii atermicheskogo zaedaniya pri granichnoi smazke," *Mashinovedenie*, no. 1, pp. 86–91, 1982.

[10] B. Kostetsky, *Trenie, smazka i iznos v mashinakh*, Kyiv: Tekhnika, 1970.

[11] B. Deryagin, "O vliyanii mikrogeometrii poverkhnosti tverdogo tela na smachivanie," *Trenie i iznos v mashinakh*, vol. 1, pp. 74–76, 1947.

[12] A. Zimon, *Adgeziya zhidkosti i smachivanie*, Moscow: Khimiya, 1974.

[13] V. Marchuk, M. Kindrachuk, Ya. Krysak, O. Tisov, O. Dukhota, and Y. Gradiskiy, "The Mathematical Model of Motion Trajectory of Wear Particle Between Textured Surfaces," *Tribology in Industry*, vol. 43, no. 2, pp. 241–246, Jun. 2021, doi: 10.24874/ti.1001.11.20.03.

[14] F. Quinci, W. Litwin, M. Wodtke, and R. van den Nieuwendijk. "A comparative performance assessment of a hydrodynamic journal bearing lubricated with oil and magnetorheological fluid," *Tribology International*, vol. 162, p. 107143, Jun. 2021, doi: 10.1016/j.triboint.2021.107143.

[15] V. Marchuk, M. Kindrachuk, O. Harmash, and V. Kharchenko, "Determining features in the wear resistance characteristics of tribocompounds with a textured hole surface under conditions of boundary friction," *Eastern-European Journal of Enterprise Technologies*, vol. 6, no. 12 (126), pp. 22–29, Dec. 2023, doi: 10.15587/1729-4061.2023.291785.

[16] A. Kovalchenko, O. Ajayi, A. Erdemir, and G. Fenske, "Friction and wear behavior of laser textured surface under lubricated initial point contact," *Wear*, vol. 271, no. 9–10, pp. 1719–1725, Jul. 2011, doi: 10.1016/j.wear.2010.12.049.

[17] U. Sudeep, R. K. Pandey, and N. Tandon, "Effects of surface texturing on friction and vibration behaviors of sliding lubricated concentrated point contacts under linear reciprocating motion," *Tribology International*, vol. 62, pp. 198–207, Mar. 2013, doi: 10.1016/j.triboint.2013. 02. 023.

[18] G. V. Tsyban'ov, V. E. Marchuk, and O. O. Mikosyanchyk, "Effect of textured dentated surfaces on 30KhGSA steel damage and life at fatigue, fretting fatigue, and fretting," *Strength of Materials*, vol. 51, no. 3, pp. 341–349, May 2019, doi: 10.1007/s11223-019-00080-x.

[19] F. Snegovsky, and I. Vinichenko, "Mekhanizm deistviya sistemy mikrokanalov pri granichnoi smazke," *Problemy trenia i iznashivaniya*, vol. 18, pp. 86–89, 1971.

[20] A. Zabolotsky, V. Ryabenko, and V. Shpinev, "Primenenie regularnogo mikrorelefa dlya povysheniya protivozadirnoi stoikosti soprajeniya s reversivnymi peremeshcheniyami detalei," *Vestnik mashinostroeniya*, no. 8, pp. 27–29, 1983.

[21] G. Sinyakov, and A. Rybikov, "Rabochii uzel mashiny dlya issledovaniya granichnogo trenia," *Problemy trenia i iznashivaniya*, no. 18, pp. 67–72, 1980.

[22] M. Pashechko, V. Marchuk, M. Kindrachuk, O. Tisov, A. Kornienko, and O. Dukhota, "Fretting-Wear mechanism of textured surfaces," *Advances in Science and Technology – Research Journal*, vol. 13, no. 3, pp. 186–191, Sep. 2019, doi: 10.12913/22998624/111966.

[23] I. C. M. F. Filho, A. C. Bottene, E. J. Silva, and R. Nicoletti, "Static behavior of plain journal bearings with textured journal - Experimental analysis," *Tribology International*, vol. 159, p. 106970, Mar. 2021, doi: 10.1016/j.triboint.2021.106970.

[24] J. Xu, K. Kato, and T. Hirayama, "The transition of wear mode during the running-in process of silicon nitride sliding in water," *Wear*, vol. 205, no. 1–2, pp. 55–63, Apr. 1997, doi: 10.1016/S0043-1648(96)07283-3.

[25] X. Wang, K. Kato, K. Adachi, and K. Aizawa, "Loads carrying capacity map for the surface texture design of SiC thrust bearing sliding in water," *Tribology International*, vol. 36, no. 3, pp. 189–197, Dec. 2002, doi: 10.1016/S0301-679X(02)00145-7.

[26] T. Klimczak and M. Jonasson, "Analysis of real contact area and change of surface texture on deep drawn steel sheets," *Wear*, vol. 179, no. 1–2, pp. 129–135, Dec. 1994, doi: 10.1016/0043-1648(94)90230-5.

[27] Q. J. Wang and Y.-W. Chung, *Encyclopedia of Tribology*. 2013. doi: 10.1007/978-0-387-92897-5.

[28] G. Boidi *et al.*, "Fast laser surface texturing of spherical samples to improve the frictional performance of elasto-hydrodynamic lubricated contacts," *Friction*, vol. 9, no. 5, pp. 1227–1241, Jan. 2021,, doi: 10.1007/s40544-020-0462-4.

[29] S. Kango, R. K. Sharma, and R. K. Pandey, "Thermal analysis of microtextured journal bearing using non-Newtonian rheology of lubricant and JFO boundary conditions," *Tribology International*, vol. 69, pp. 19–29, Aug. 2013, doi: 10.1016/j.triboint.2013.08.009.

[30] Y. Han *et al.*, "Effects of shaft axial motion and misalignment on the lubrication performance of journal bearings via a fast mixed EHL computing technology," *Tribology Transactions*, vol. 58, no. 2, pp. 247–259, Oct. 2014, doi: 10.1080/10402004.2014.962207.

[31] V. Ye. Marchuk, I. F. Shulha, O. I. Shulha, O. Ye. Plyusnin, "Device for Creating a Relief of Depressions on a Flat Friction Surface to Retain Lubricants," Ukraine Patent 13762, Apr. 17 2006.

[32] V. Ye. Marchuk, I. F. Shulha, B. A. Lyashenko, G. V. Tsybanyov, A. V. Rutkovsky, V. V. Kalinichenko, "Method for Obtaining Relief Wear-Resistant Nitrided Layers of Steel Parts," Ukraine Patent 44643, Oct. 12 2009.